

*Supplementary Informations*

# Functional diversity of mouse dLGN neurons and modulation of their encoding properties by superior colliculus.

## Supplementary Methods

*Quantification and statistical*

### 1. Preprocessing and spike sorting

Electrical signals were sampled at 20 kHz. Spike activity was high pass filtered at 300 Hz. We used 4 times the number of standard deviation in the mean of the peak height histogram to threshold the spike signals. Multi-unit spikes were initially clustered using K-means in Offline sorter (Plexon Inc., USA) and manually grouped similar clusters if necessary.

Units were included for analysis only if they met the following quality criteria: (1) threshold-crossing waveforms, aligned to the positive peak, formed a clearly separated cluster; (2) waveform shape remained stable over time; and (3) interspike intervals showed no refractory-period violations[1].

For paired analyses in the SC silencing experiments, pre- and post-muscimol recordings were concatenated and spike-sorted together to ensure consistent unit identification across the two epochs. The two segments were then analyzed separately. Neurons were excluded from paired analysis if they lost their receptive field after muscimol injection or if their mean firing rate in the post-injection condition was below 1 Hz.

### 2. Construction of the feature matrix

Before clustering, we used non-negative matrix factorization (NNMF) to obtain a low-dimensional, non-negative representation of dLGN population responses. For each data set, responses of  $N$  neurons over  $M$  time bins were arranged in a non-negative matrix  $A$  [2]. Given a desired number of components  $k$ , NNMF approximates  $A$  as the product of two low-rank non-negative matrices:

$$A \approx UV^T$$

where  $U$  is an  $N \times k$  matrix containing the loading of each neuron on each component, and  $V$  is an  $M \times k$  matrix containing the temporal profile of each component. All entries of  $A$ ,  $U$ , and  $V$  were constrained to be non-negative.

The factors  $U$  and  $V$  were obtained by minimizing the squared reconstruction error under these non-negativity constraints:

$$\min_{U, V \geq 0} \|A - UV^T\|_F^2$$

To determine the number of NMF components, we used a mean-squared-error (MSE) based model selection procedure[3]. For each fit we computed the reconstruction mean squared error,

$$MSE^{(r)}(k) = \frac{1}{NM} \|A - U^{(r)}(V^r)^T\|_F^2$$

The MSE for rank  $k$  was then obtained by averaging over random initializations,

$$MSE(k) = \frac{1}{R} \sum_{r=1}^R MSE^{(r)}(k)$$

Candidate ranks from  $k = 1$  to 50 were evaluated. For each rank, the factorization was repeated 200 times. In each repeat, 10% of matrix entries were randomly held out as a test set, and the remaining entries were used for model fitting. NMF was initialized using NNDSVD and optimized with a maximum of 1000 iterations. For each repeat, the MSE was computed separately on training and held-out test entries. Mean train and test MSE values were then averaged across repeats, and 95% confidence intervals were estimated from the empirical distributions across repeats. The optimal number of components was defined as the smallest rank whose mean test MSE was within 5% of the minimum mean test MSE across all tested ranks, in order to favor a parsimonious representation while avoiding overfitting. All downstream clustering analyses used the NMF feature matrix  $U$  at the selected rank.

### 3. Clustering

All neurons were first partitioned into three functional classes, direction selective (DS), orientation selective (OS), and non-selective. All subsequent clustering analyses were performed separately within each class. Below we describe the pipeline for the DS population; OS and non-selective were treated identically and used the same hyper-parameters.

We collected multiple NMF-derived or functional feature sets. Each feature set  $g = 1, \dots, G$  was stored as a matrix

$$X^{(g)} \in \mathbb{R}^{N \times F_g}$$

where  $X^{(g)}$  contains the features for set  $g$ ,  $N$  denote the number of neurons,  $F_g$  is the number of features in that set. Upon loading, matrices were re-oriented to this  $N \times F_g$  convention.

Each feature set was clustered independently using a Gaussian mixture model (GMM) with diagonal covariance matrices:

$$p(x) = \sum_{i=1}^K \phi_i N(x | \mu_i, \sigma_i)$$

$$K \in [2, \min(50, F_g + 1)]$$

$$N(x | \mu_i, \sigma_i) = \frac{1}{\sigma_i \sqrt{2\pi}} \exp\left(-\frac{(x - \mu_i)^2}{2\sigma_i^2}\right)$$

$$\frac{1}{\sigma_i \sqrt{2\pi}}$$

For each  $K$ , the expectation–maximization algorithm was initialized  $n_{init} = 1000$  times with random starting points, a maximum of 200 iterations, and a covariance regularization term to improve numerical stability. For each  $K$ , the model with the lowest Bayesian information criterion (BIC) was retained[4]. The BIC was defined as:

$$BIC = -2 \ln L + k \ln n$$

where  $L$  is the maximized likelihood of the model,  $k$  is the number of free parameters, and  $n$  is the number of neurons. For each feature set  $g$ , this procedure yielded an integer label  $\ell_i^{(g)}$  for every neuron  $i = 1, \dots, N$ , which was used for downstream consensus clustering.

Local labels from all feature sets were stacked column-wise into an integer label matrix:

$$L \in \mathbb{Z}^{N \times G}$$

Each column was one-hot encoded and the resulting binary vectors were concatenated across feature sets to form a design matrix  $H$ . Columns of  $H$  were standardized to zero mean and unit variance using z-score normalization. On the embedding  $Z$  we fitted diagonal-covariance GMMs with

$$K \in [2, 50]$$

For each  $K$ , we recorded the corresponding BIC value. Final cluster number  $K$  is at which the second finite difference of the BIC reached its maximum.

To assess robustness of the final partition, we fixed  $K$  and refitted the GMM ( $R = 100$  times) with different random seeds. Let  $\ell_i^{(r)}$  denote the label of neuron  $i$  obtained in restart  $r$ . We defined the consensus matrix:

$$C_{ij} = \frac{1}{R} \sum_{r=1}^R [\ell_i^{(r)} = \ell_j^{(r)}], \quad R = 100$$

where  $C_{ij}$  is the fraction of restarts in which neurons  $i$  and  $j$  were assigned to the same cluster.

Cluster stability was further quantified using two summary indices derived from the consensus matrix  $C$  [5]. The average pairwise consensus among members of cluster  $k$  :

$$Intra\ stability_k = \frac{\sum_{i \neq j; i, j \in I_k} C_{ij}}{|I_k| (|I_k| - 1)}$$

Where  $I_k$  denotes the index set of neurons assigned to cluster  $k$  in the final solution, and  $|I_k|$  its cardinality.  $Inter\ separation_k$  measures how rarely neurons in cluster  $k$  co-cluster with neurons outside  $k$

$$Inter\ separation_k = 1 - \text{mean}(C_{ij}; i \in I_k, j \notin I_k)$$

To visualize the relative organization of cluster centers in a low-dimensional space, t-distributed stochastic neighbor embedding (t-SNE) was performed with two output dimensions, a perplexity of 5, PCA initialization, and random seed 42.

#### 4. Quantification of functional properties

To quantitatively describe the functional properties of dLGN neurons, we derived a set of scalar indices that summarize tuning to motion direction and orientation, temporal and spatial frequency, stimulus size, surround suppression, contrast, color, and response dynamics. Below we describe how these indices were computed from baseline-subtracted responses. All analyses were performed in Python.

For each dLGN neuron for each velocity, we quantified direction and orientation selectivity from responses to drifting gratings and static grating. For each direction  $\theta_k$  ( $k = 1, \dots, 8$ ), the trial-averaged response  $R_k$  was computed as the baseline-subtracted mean response over the stimulation window. From the baseline-subtracted trace  $R_k(t)$ , we obtained a positive and a negative response component by averaging separately over time points with  $P_k$  as the mean of  $R_k(t)$  over all time points with  $R_k(t) > 0$ , and  $N_k$  as the mean of  $R_k(t)$  over all time points with  $R_k(t) < 0$ .

To quantify direction tuning, we calculated separate direction selectivity indices for positive and negative responses as the normalized length of the response-weighted vector sum over all directions:

$$\begin{aligned} DSI_{pos} &= \frac{\sqrt{(\sum_k P_k \sin \theta_k)^2 + (\sum_k P_k \cos \theta_k)^2}}{\sum_k P_k} \\ DSI_{neg} &= \frac{\sqrt{(\sum_k N_k \sin \theta_k)^2 + (\sum_k N_k \cos \theta_k)^2}}{\sum_k N_k} \\ OSI_{pos} &= \frac{\sqrt{(\sum_k P_k \sin 2\theta_k)^2 + (\sum_k P_k \cos 2\theta_k)^2}}{\sum_k P_k} \\ OSI_{neg} &= \frac{\sqrt{(\sum_k N_k \sin 2\theta_k)^2 + (\sum_k N_k \cos 2\theta_k)^2}}{\sum_k N_k} \end{aligned}$$

This procedure was applied independently for each temporal and spatial frequency condition, yielding  $DSI_{pos}$ ,  $DSI_{neg}$ ,  $OSI_{pos}$ , and  $OSI_{neg}$  for every neuron and stimulus condition. For each neuron and stimulus condition, we further assessed the significance of DSI/OSI using a shuffle-based permutation test, in which direction labels were randomly permuted across trials to generate

a null distribution of indices. Neurons with all four indices  $\leq 0.1$  were classified as non-selective. If at least one index exceeded 0.1, neurons were assigned to a single category according to the following priority, and we defined a hierarchy  $DSI_{pos}$ ,  $DSI_{neg}$ ,  $OSI_{pos}$ , and  $OSI_{neg}$  [6]. This hierarchy was used to resolve mixed-selectivity cases and avoid double assignment according to previous studies [6, 7, 8].

To quantify the selectivity to On/Off contrast, we calculated the contrast selectivity index (CSI):

$$CSI = \frac{R_{ON} - R_{OFF}}{R_{ON} + R_{OFF}}$$

where  $R_{ON}$  and  $R_{OFF}$  are the peak responses to flashing full field white and black stimulus in chirp stimulus, respectively.

To quantify the selectivity to the flash frequency, we calculated the frequency selectivity index (FSI):

$$FSI = \frac{R_{highf} - R_{lowf}}{R_{highf} + R_{lowf}}$$

where  $R_{lowf}$  and  $R_{highf}$  are the peak responses in the first 3s and last 3s temporal windows of the frequency-modulated stimulus in chirp stimulus.

To quantify the selectivity to the flash amplitude changes, we calculated the amplitude selectivity index (ASI):

$$ASI = \frac{R_{higha} - R_{lowa}}{R_{higha} + R_{lowa}}$$

where  $R_{lowa}$  and  $R_{higha}$  are the peak responses in the first 3s and last 3s temporal windows of the amplitude-modulated stimulus in chirp stimulus.

To quantify the frequency preference, we calculated the frequency preference index (FPI):

$$FPI = \frac{f_{peak} - f_{min}}{f_{max} + f_{min}}$$

where  $f_{peak}$  is the frequency at which the frequency response metric  $R_f$  reached its maximum, and  $f_{min}$  and  $f_{max}$  are the lower and upper bounds of the sweep (2 and 8 Hz, respectively) in chirp stimulus.

To quantify the amplitude changes preference, we calculated the amplitude changes preference index (API):

$$API = \frac{A_{peak} - A_{min}}{A_{max} + A_{min}}$$

where  $A_{peak}$  is the amplitude at which the amplitude response metric  $R_a$  reached its maximum, and  $A_{min}$  and  $A_{max}$  are the lower and upper bounds of the ramp (0 and 1, respectively) in chirp stimulus.

To quantify the extent of frequency selectivity, we defined the frequency selectivity window

index (FSWI):

$$FSWI = \frac{f_{up} - f_{low}}{f_{up} + f_{low}}$$

where  $f_{up}$  and  $f_{low}$  denote the upper and lower temporal frequencies at half-maximal response, determined by the two intercept points of the 50% peak response level in chirp stimulus.

To quantify the extent of the amplitude selectivity, we calculated the amplitude selectivity window index (ASWI):

$$ASWI = \frac{A_{up} - A_{low}}{A_{up} + A_{low}}$$

where  $A_{up}$  and  $A_{low}$  denote the upper and lower amplitude changes at half-maximal response, determined by the two intercept points of the 50% peak response level in chirp stimulus.

To quantify the magnitude of phase delay during the chirp amplitude segment, we band-pass filtered the baseline-subtracted response trace (1.5–2.5 Hz) in the temporal windows of the amplitude-modulated stimulus in chirp stimulus and extracted the instantaneous phase using the Hilbert transform. We calculated the phase delay index (PDI):

$$\Delta\varphi(t) = \arg(e^{i(\varphi_r(t) - \varphi_{stim}(t))})$$

$$\bar{\varphi} = \arg\left(\frac{1}{T} \sum_{t=1}^T e^{i\Delta\varphi(t)}\right)$$

$$PDI = \frac{|\bar{\varphi}|}{\pi}$$

where  $\varphi_r(t)$  is the instantaneous neural phase (Hilbert transform of the 1.5–2.5 Hz band-pass-filtered trace),  $\varphi_{stim}(t)$  is the stimulus reference phase ( $f = 2$  Hz),  $T$  is the number of time samples within the analyzed window.

To assess potential S-cone or M-cone mediated preference, we calculated the blue–green index (BGI):

$$BGI = \frac{R_{blue} - R_{green}}{R_{blue} + R_{green}}$$

where  $R_{blue}$  is the responses to blue stimuli, and  $R_{green}$  is the responses to green stimuli.

To quantify the selectivity to the speed of white looming stimuli, we defined a white speed selectivity index (WSSI):

$$WSSI = \frac{R_{white(max\ speed)} - R_{white(min\ speed)}}{R_{white(max\ speed)} + R_{white(min\ speed)} + C_{white}}$$

where  $R_{white(max\ speed)}$  and  $R_{white(min\ speed)}$  denote the responses to white looming stimuli presented at the maximal and minimal speed.  $\mu_{i,s}^W$  represent the mean responses of the  $i$  neuron to the white looming stimuli, at the  $s$  speed condition, with the mean computed over the corresponding

valid analysis window for that speed condition.  $c_{white}$  denotes the mean of  $\mu_{i,s}^W$  pooled across all neurons and all speed conditions, and was included as a stabilizing term in the denominator.–

To quantify the selectivity to the speed of white looming stimuli, we defined a black speed selectivity index (BSSI):

$$BSSI = \frac{R_{black(max\ speed)} - R_{black(min\ speed)}}{R_{black(max\ speed)} + R_{black(min\ speed)} + C_{black}}$$

where  $R_{black(max\ speed)}$  and  $R_{black(min\ speed)}$  denote the responses to black looming stimuli presented at the maximal and minimal speed.  $\mu_{i,s}^B$  represent the mean responses of the  $i$  neuron to the white looming stimuli, at the  $s$  speed condition, with the mean computed over the corresponding valid analysis window for that speed condition.  $c_{black}$  denotes the mean of  $\mu_{i,s}^B$  pooled across all neurons and all speed conditions, and was included as a stabilizing term in the denominator.

To quantify the tuning of responses to white looming speed, we defined a white looming tuning index (WLTi):

$$WLTi = \frac{R_{white(max\ speed)} - R_{white(min\ speed)}}{\sum_{i=1}^5 |R_{i+1} - R_i|}$$

Where  $R_i$  denote the baseline-subtracted mean response to white looming at the  $i$  speed level, with speeds ordered from lowest to highest

To quantify the tuning of responses to black looming speed, we defined a black looming tuning index (BLTI):

$$BLTI = \frac{R_{black(max\ speed)} - R_{black(min\ speed)}}{\sum_{i=1}^5 |R_{i+1} - R_i|}$$

Where  $R_i$  denote the baseline-subtracted mean response to black looming at the  $i$  speed level, with speeds ordered from lowest to highest

To compare speed selectivity between white and black looming stimuli, we defined a speed selectivity index (SSI) based on the relative difference between WSSI and BSSI:

$$SSI = \frac{WSSI - BSSI}{WSSI + BSSI}$$

where  $WSSI$  and  $BSSI$  are white and black speed selectivity index.

**Figure S1**

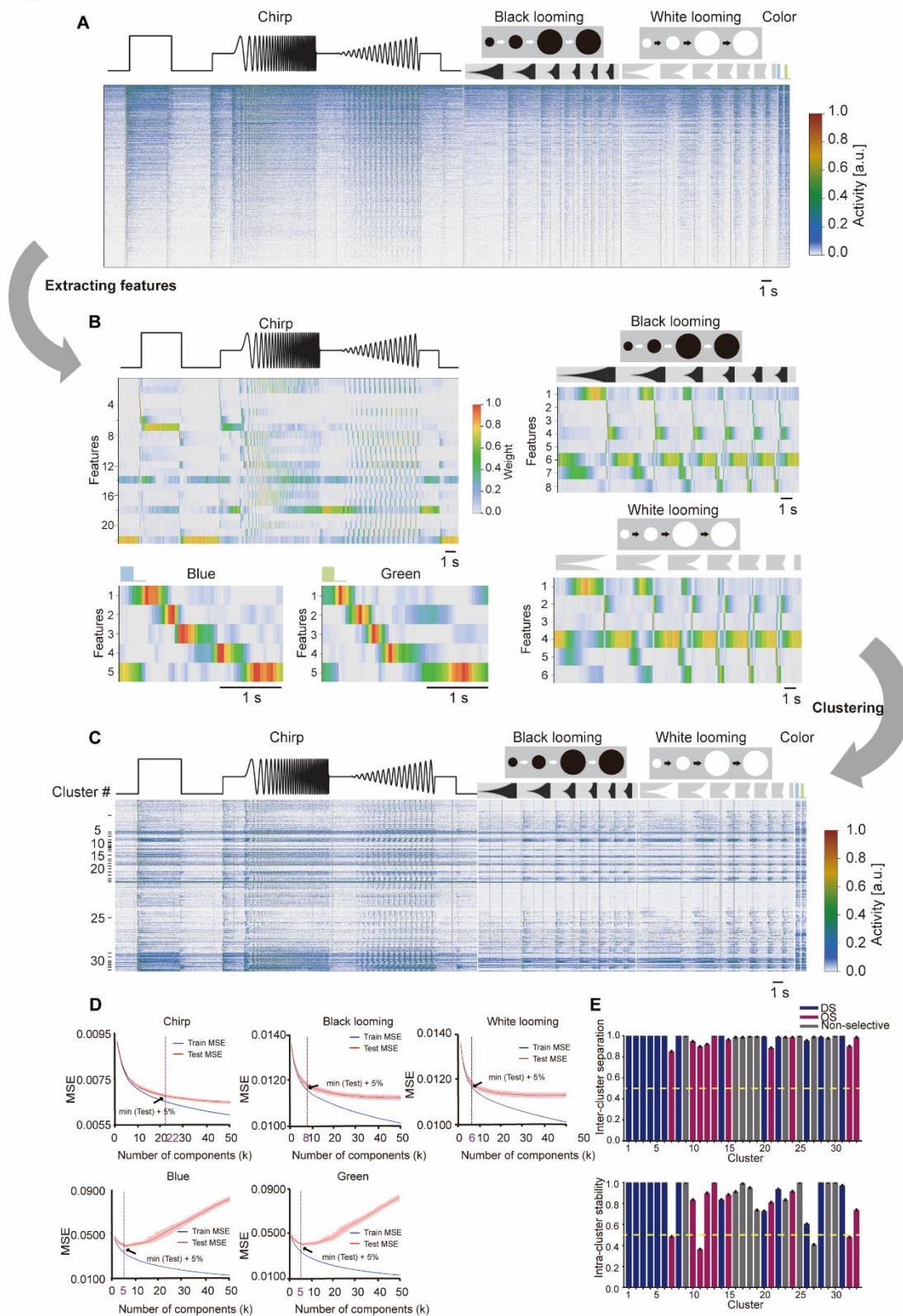


**Fig S1. Feature extraction and data-driven clustering workflow.**

(A) Paradigm-wise response matrix (example shown) assembled for each neuron prior to feature extraction.

(B) NNMF-based feature extraction. Responses from each paradigm (chirp, black looming, white looming, blue, and



green) were decomposed and summarized into paradigm-specific feature sets, shown as neuron-by-feature heatmaps (rows, neurons; columns, feature dimensions). Features were then concatenated across paradigms to form a unified feature vector for each neuron.

**(C)** Global clustering performed on the concatenated feature space (66 dimensions per neuron, 22 from ‘chirp’, 8 from black looming, 6 from white looming, 5 each from blue and green, 10 each from DSI and OSI) to generate the final neuron  $\times$  feature matrix used for downstream analyses; clusters are displayed in a fixed dendrogram leaf order (33 clusters).

**(D)** Cross-validated NMF reconstruction error as a function of the number of components ( $k$ ) for chirp, black looming, white looming, blue, and green. Blue curves denote training mean squared error (MSE) and red curves denote test MSE (shaded band, variability across cross-validation folds). The selected model order (purple dashed line) was defined as the smallest  $k$  whose test MSE was within 5% of the minimum test MSE ( $\min(\text{test}) + 5\%$  criterion).

**(E)** Per-cluster assessment of clustering robustness across the 33 dLGN functional clusters. Cluster-wise inter-cluster separation (top) and intra-cluster stability (bottom) are shown for all 33 clusters, ordered according to the dendrogram in Fig. 2B. Bar colors indicate cluster class identity (DS, blue; OS, magenta; non-selective, gray). The dashed horizontal line marks an acceptance threshold of 0.5. All clusters showed inter-cluster separation values above 0.5, indicating good separation from other clusters. In contrast, five clusters showed intra-cluster stability values below 0.5, indicating relatively lower within-cluster consistency. These lower-stability clusters are marked with star symbols in Fig. 2B.

**Figure S2**

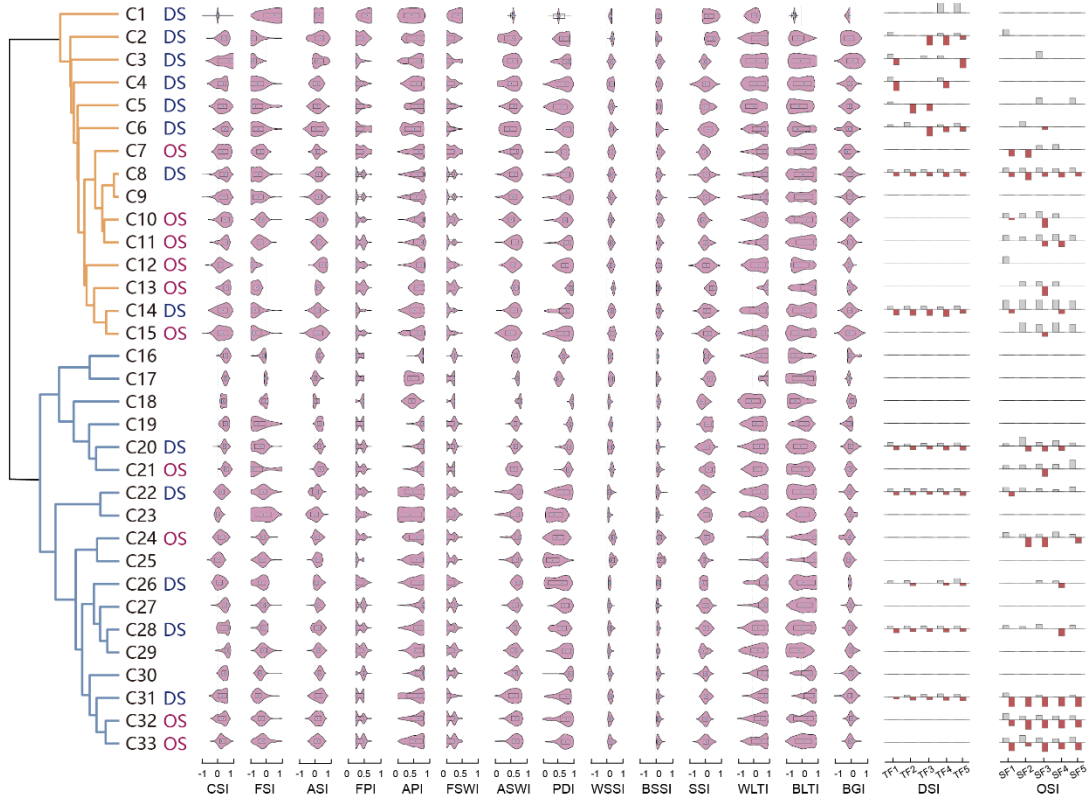


**Fig S2. Cluster-wise distributions of functional indices in dLGN**

Violin plots showing the within-cluster distributions of functional indices across the 33 data-driven dLGN clusters (DS/OS annotations at left). For each cluster and index, the violin depicts the full distribution across units, with the central marker indicating the median and the box indicating the interquartile range (IQR). Right panels summarize cluster-level direction/orientation selectivity metrics (DSI/OSI) across temporal and spatial frequency conditions, with gray bars indicating positive DSI/OSI and red bars indicating negative DSI/OSI. (TF1–TF5 denote 1, 2, 4, 8, and 15 Hz, respectively; SF1–SF5 denote 0.02, 0.04, 0.08, 0.16, and 0.32 cpd, respectively)

**Figure S3**

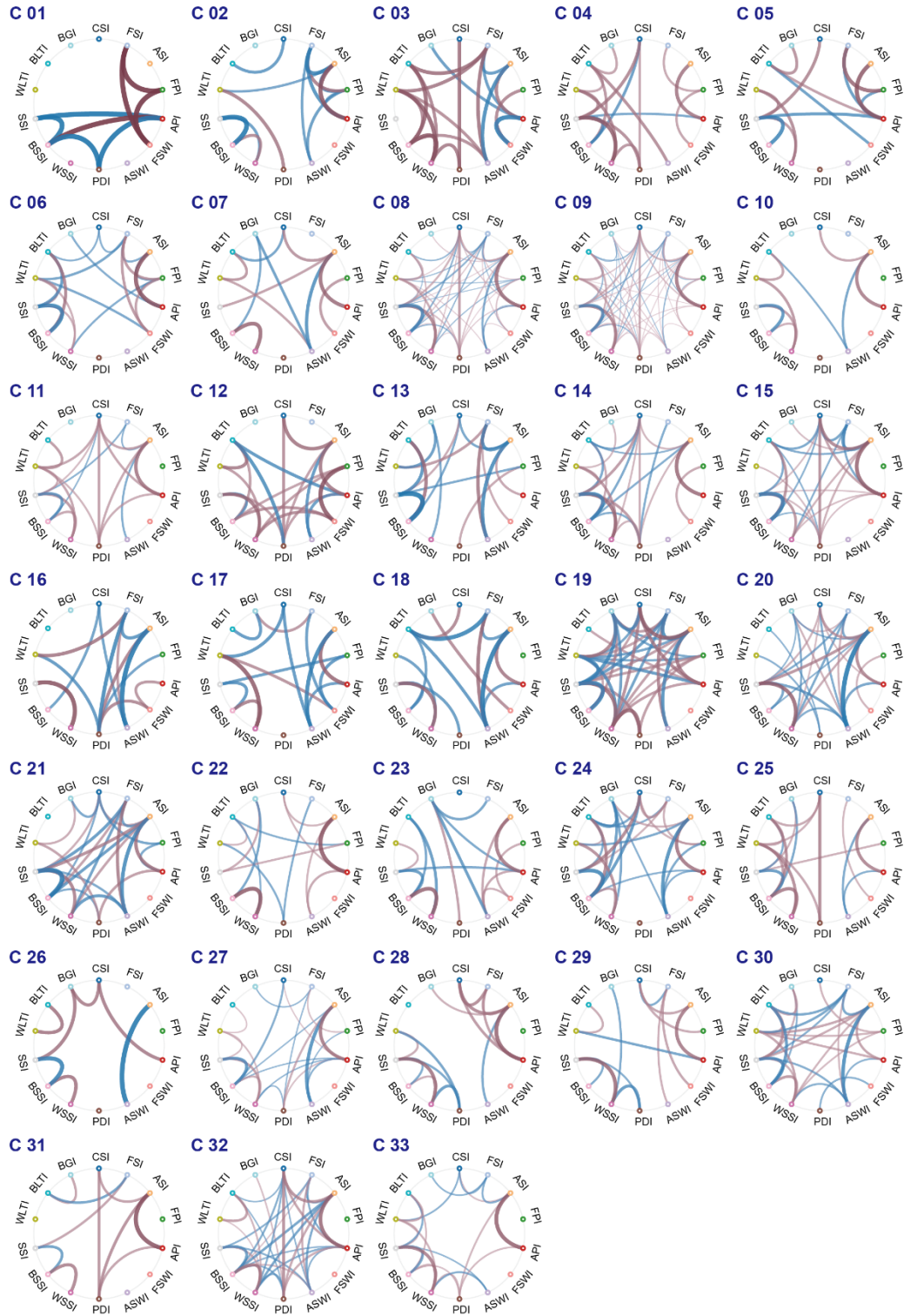


**Fig S3. Inter-index correlations within dLGN clusters.**

Chord diagrams showing significant pairwise correlations among 14 functional indices (CSI, FSI, ASI, FPI, API, FSWI, ASWI, PDI, WSSI, BSSI, SSI, WLTi, BLTi, and BGI) rendered separately for each of the 33 clusters. Blue edges denote negative correlations and red edges denote positive correlations; edge thickness scales with  $|R|$ . Correlations are shown only when passing the significance threshold and multiple-comparison correction.

**Figure S4**

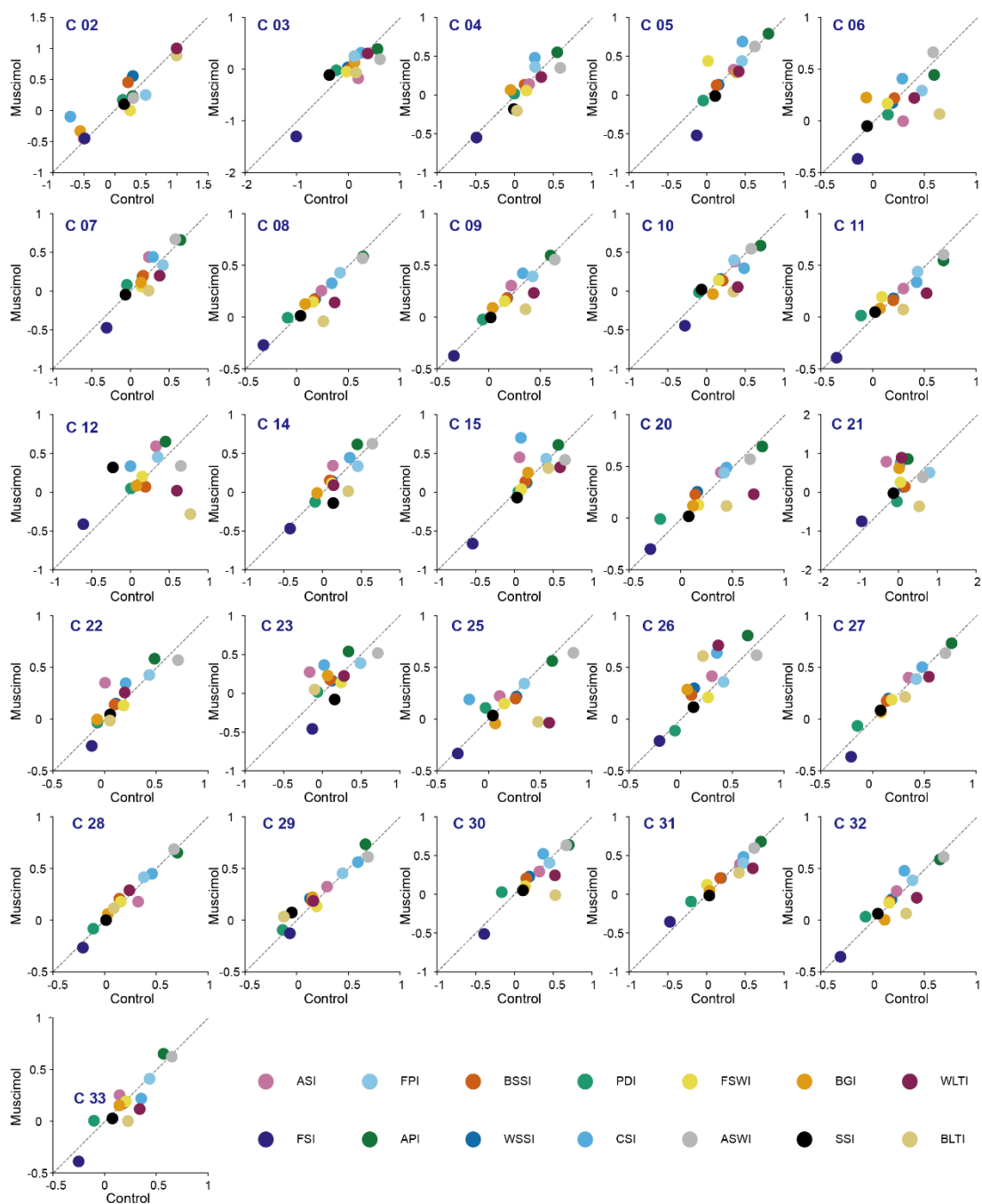


**Fig S4. Paired cluster-level changes of functional indices following SC inactivation.**

Per-cluster scatter plots compare the mean value of each functional index under Control (x-axis) versus Muscimol (y-axis) for clusters that contained paired units across conditions (only clusters with sufficient paired samples are shown). Each dot corresponds to one of 14 functional indices (CSI, FSI, ASI, FPI, API, FSWI, ASWI, PDI, WSSI, BSSI, SSI, WLTl, BLTI, and BGI). The dashed line denotes unity ( $y = x$ ); points above/below the line indicate increases/decreases under muscimol.

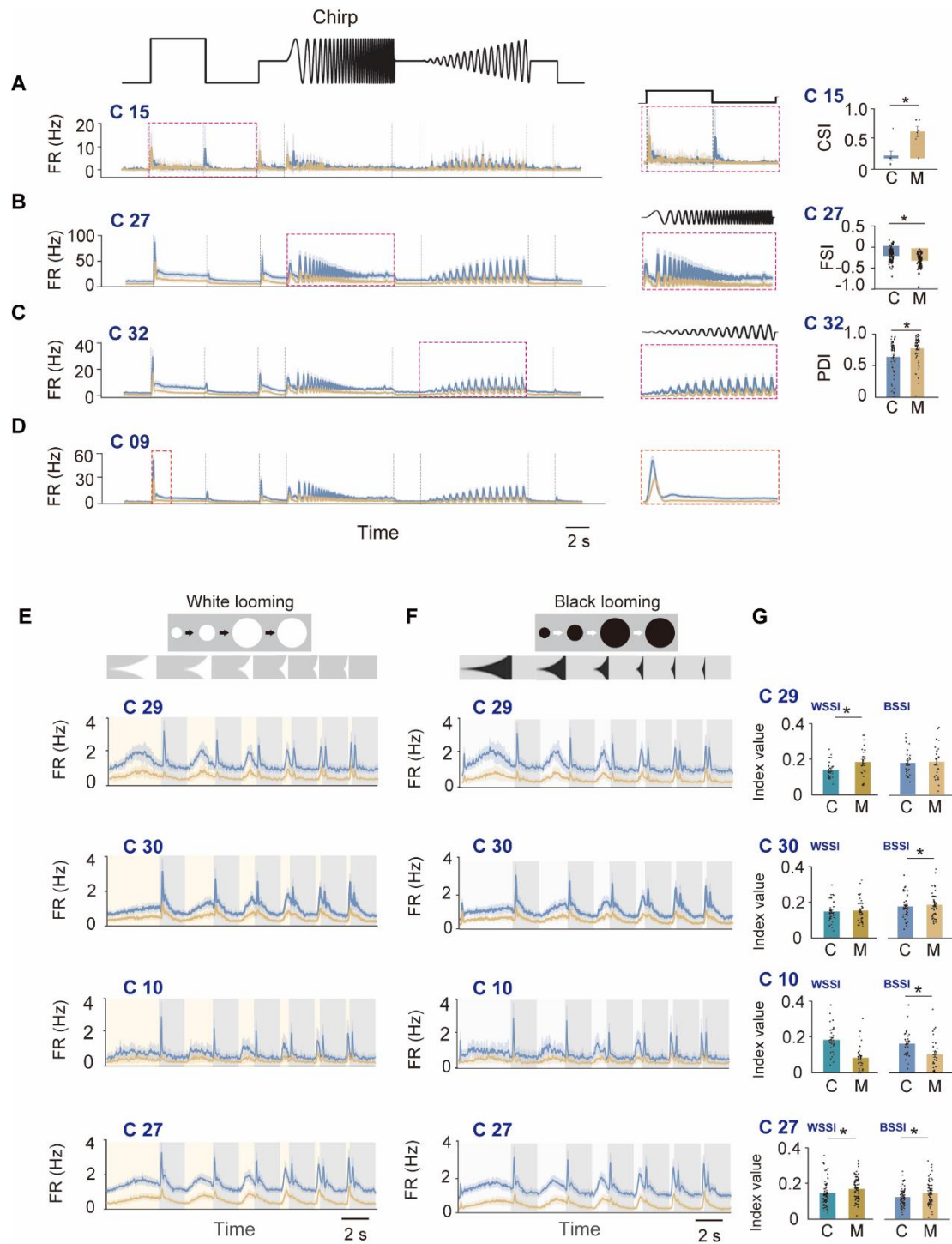


**Fig S5. Representative clusters showing index changes following SC inactivation.**

(A–D) Example clusters with significant Control–Muscimol differences in chimp-derived indices: C15 (A; CSI), C27 (B; FSI), C32 (C; PDI) and C09 (D). For each row, left: trial-averaged firing-rate trace across the full chimp epoch (Control, blue; Muscimol, orange). Middle: magnified view of the response segment used for index quantification (analysis window indicated). Right: paired within-unit index values (C, Control; M, Muscimol).

(E–G) Looming examples from clusters C29, C30, C10, and C27. (E) Trial-averaged responses to white looming and (F) to black looming; shaded intervals denote stimulus epochs (yellow, white looming; white, black looming; gray, inter-stimulus). (G) Paired comparisons of looming-derived speed selectivity indices (WSSI and BSSI) for the same clusters. Data were presented as mean  $\pm$  SEM. Statistical significance was determined using BH-FDR

correction (FDR<0.05). \* $p < 0.05$ .

## Figure S6

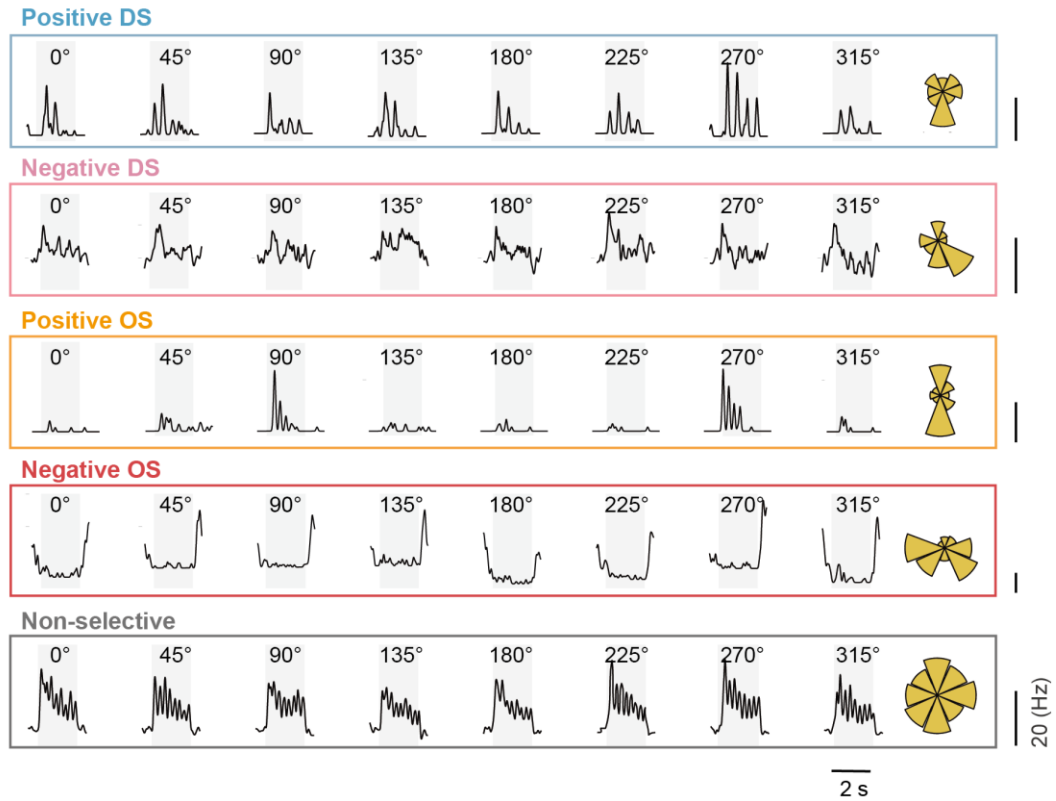


**Fig S6. Representative examples of direction- and orientation-selective dLGN units.**

Example baseline-subtracted firing-rate traces to drifting gratings moving in eight directions (0°–315°; 45° steps) are shown for five response classes (positive DS, negative DS, positive OS, negative OS, and non-selective). Each row corresponds to one example unit; shaded regions mark the 2s stimulus epoch for each direction. Right, polar plots summarize direction/orientation tuning, where the radius for each direction represents the baseline-subtracted response integral over the stimulus window.

**Figure S7**

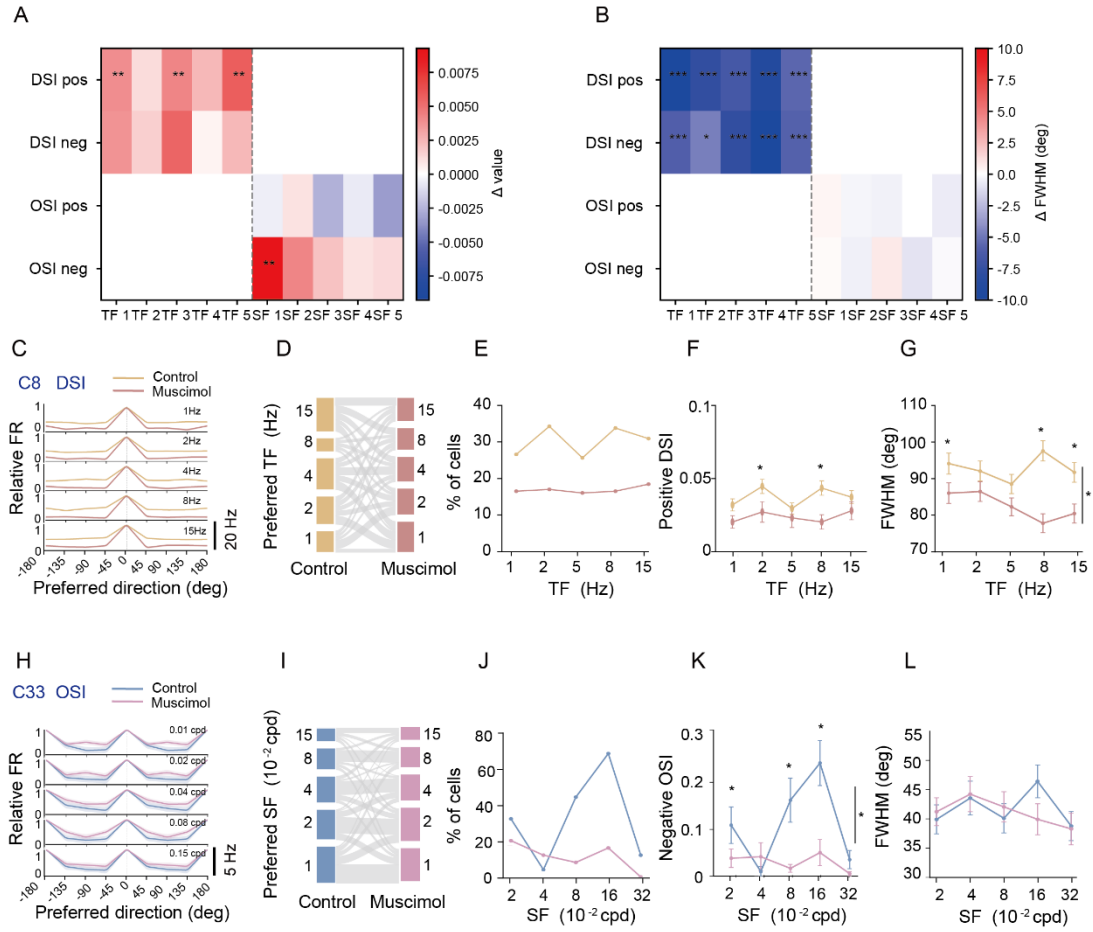


**Fig S7. SC inhibition modulates dLGN direction/orientation selectivity metrics.**

Common definitions for A-B: TF1–TF5 denote 1, 2, 4, 8, and 15 Hz; SF1–SF5 denote 0.02, 0.04, 0.08, 0.16, and 0.32 cpd.

(A) Heatmap of condition-induced changes in selectivity magnitude ( $\Delta$  = Muscimol – Control) for positive and negative DSI (TF1–TF5) and positive and negative OSI (SF1–SF5) across the 989 paired dLGN units.

(B) Heatmap of corresponding changes in tuning width ( $\Delta$ FWHM; Muscimol – Control) for positive/negative DS and OS across TF and SF conditions. (TF1–TF5 denote 1, 2, 4, 8, and 15 Hz, respectively; SF1–SF5 denote 0.02, 0.04, 0.08, 0.16, and 0.32 cpd, respectively)

(C–L) An example DS-enriched cluster (C8) quantified across temporal-frequency (TF) conditions. (F–J) An example OS-enriched cluster (C33) quantified across spatial-frequency (SF) conditions. Control and muscimol measurements are paired within the same units.

(C, H) Direction/orientation tuning curves at each TF (A) or SF (F)

(D, I) Sankey diagram showing within-unit shifts in the preferred TF (B) or preferred SF (G) bin from control to muscimol.

(E, J) Fraction of units meeting the selectivity criterion at each TF (C) or SF (H) (DSI/OSI > 0.1).

(F, K) Mean selectivity index (DSI in (D); OSI in (I)) at each TF/SF.

(G, L) Full width at half maximum (FWHM) computed from the peak-aligned, smoothed tuning curves.

Data were presented as mean  $\pm$  SEM. \* $p$  < 0.05, \*\* $p$  < 0.01, \*\*\* $p$  < 0.001.

## References

[1] Hill DN, Mehta SB, Kleinfeld D. Quality metrics to accompany spike sorting of



- extracellular signals. *J Neurosci.* 2011; 31: 8699–8705.  
<https://doi.org/10.1523/JNEUROSCI.0971-11.2011>
- [2] Lee DD, and Seung, H.S. Learning the parts of objects by non-negative matrix factorization. *Nature.* 1999; 401: 788–791. <https://doi.org/10.1038/44565>
- [3] Williams AH, Kim TH, Wang F, Vyas S, Ryu SI, Shenoy KV, et al. Unsupervised Discovery of Demixed, Low-Dimensional Neural Dynamics across Multiple Timescales through Tensor Component Analysis. *Neuron.* 2018; 98: 1099–1115 e1098.  
<https://doi.org/10.1016/j.neuron.2018.05.015>
- [4] Fraley C, Raftery AE. Model-Based Clustering, Discriminant Analysis, and Density Estimation. *Journal of the American Statistical Association.* 2002; 97: 611–631.  
<https://doi.org/10.1198/016214502760047131>
- [5] Sonpatki P, Shah N. Recursive Consensus Clustering for novel subtype discovery from transcriptome data. *Sci Rep.* 2020; 10: 11005. <https://doi.org/10.1038/s41598-020-67016-3>
- [6] Mullner FE, Roska B. Individual thalamic inhibitory interneurons are functionally specialized toward distinct visual features. *Neuron.* 2024; 112: 2765–2782 e2769.  
<https://doi.org/10.1016/j.neuron.2024.06.001>
- [7] Chen H, Liu X, Tian N. Subtype-dependent postnatal development of direction- and orientation-selective retinal ganglion cells in mice. *J Neurophysiol.* 2014; 112: 2092–2101.  
<https://doi.org/10.1152/jn.00320.2014>
- [8] Laniado DD, Maron Y, Gemmer JA, Sabbah S. A spherical code of retinal orientation selectivity enables decoding in ensembled and retinotopic operation. *Cell Rep.* 2025; 44: 115373. <https://doi.org/10.1016/j.celrep.2025.115373>